

## **Finite Element Analysis of an Outer Rotor Permanent Magnet Brushless DC Generator**

**Yazid Kraimeen<sup>1</sup>, Ibrahim Al-Adwan<sup>2</sup> and Munaf S. N. Al-Din<sup>3</sup>**

<sup>1&3</sup>*Department of Electrical Engineering  
Tafela Technical University, Tafela, Jordan,  
E-mail: yazidkraimeen@yahoo.com, msnaldin2001@yahoo.com*

<sup>2</sup>*Mechatronics Engineering Department  
Faculty of Engineering Technology  
Al Balq'a Applied University, Amman, Jordan,  
Ibrahim.aladwan@yahoo.com*

### **Abstract**

The Permanent Magnet Brushless dc generator is a simple and robust machine, which is found suitable generator for wind power generation and hybrid and electrical vehicles applications. This paper presents the steady-state performance of a small outer rotor (spindle) permanent magnet brushless DC generator. To evaluate the machine performance, two types of analysis, namely numerical technique and experimental study have been utilized. In the numerical analysis the time-stepping finite element analysis is employed, where as in the experimental study, a proto-type motor has been used and tested. The calculated results compare favorably with the test results.

### **Introduction**

Recently the demands for clean DC power generation for stand-alone electrical power generation and propulsion systems are increasing rapidly since the natural energy sources are limited and they are the main source of pollution. Furthermore, DC power source has many applications in industry such as AC motor drive, energy storage, chemical electrolysis and etc. High efficiency, high power density, compact, lightweight low maintenance and easy control are very important factors for the development for such systems [1-2]. The developments of power electronics converters and cost-effective DSP processors made Permanent Magnet (PM) Brushless DC (BLDC) machines to be well-suited for such applications [3]. As compared with other generators, the PM BLDC generator has many advantages; it is lightweight, it has a compact design and low maintenance because it has a magnetic source inside itself. With the inherent advantages of the PM BLDC generator,

additional increases in power density can be expected by the advanced control techniques, resulting in considerable reduction of weight and volume [4].

It is well known that, electrical power generated by the permanent magnet generator is an AC power and has variable amplitude and frequency. Therefore, additional conditioning is required for the generation of DC power. Many types of power electronic converters were introduced to find appropriate and inexpensive solutions to the problem of electricity conditioning; the results have been promising [5]. In the AC-DC architecture, the structure of a generator connected with a rectifier is very popular. Especially for certain applications like aircraft and vehicles, power density and efficiency is critical. It's desirable to improve the overall efficiency and power density in the generator and rectifier system [6-7].

It is widely acknowledged that simulation is an effective tool in the design and analysis of electrically driven machine systems. The analysis and design of complex electrical drive systems such as PM machines is usually done utilizing modern simulation software which can provide accurate predictions of the system's behavior in reality [8-9]. It should be noted that, the analysis and design of such drives involves taking into consideration conflicting requirements from the point of view of electromagnetic, power electronics, control and mechanical design aspects. Therefore, special analysis and design techniques need to be addressed in order to optimize those drives for brushless applications. The time stepping finite element method (FEM) has proved to be particularly flexible, reliable and effective in the analysis and synthesis of power-frequency electromagnetic and electromechanical devices. [10-12].

In this paper the simulation of PM BLDC generator using time stepping FEM will be presented and is compared with those obtained from a small outer rotor PM generator prototype. The comparison between the results obtained from the FE model and those obtained experimentally shows the validity of the FEM to analyze PM BLDC generators.

### **Finite Elements Modeling of PM BLDC Generator**

The PM BLDC generator used in this investigation which its cross-sectional view is shown in figure 1, is modeled in a two dimensional domain. The Maxwell equations and the time stepping FEM are used to formulate the magnetic field behavior of the generator. The formulation uses the magnetic vector potential as a variable and the Galerkin method to obtain the set of equations that will be solved numerically. When applying Maxwell's equations a diffusion equation of the following form will be obtained [9, 11]:

$$\nabla \times (\nu \nabla \times \mathbf{A}) = \sigma \frac{\partial \mathbf{A}}{\partial t} - \mathbf{J}_z + \nabla \times \mathbf{M}_o \quad (1)$$

Where;  $\mathbf{A}$  is the axial component of the magnetic vector potential,  $\nu$  is the reluctivity of the material;  $\sigma$  is the conductivity of the material,  $\mathbf{J}_z$  applied current density and  $\mathbf{M}_0$

the magnetization vector . The  $\sigma \frac{A}{\partial t}$  represents the induced eddy currents.

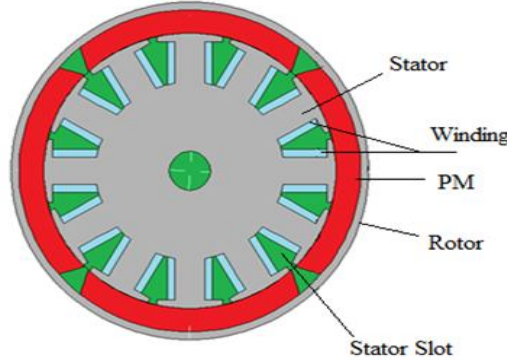


Figure (1): cross-sectional view of the PM BLDC generator.

The time-stepping FEM method solves generator steady-state and transient performance with each time-step corresponding to a constant mechanical angle of rotor movement. The sliding surface method is used to model the air gap elements [13]. In the model equations, the velocity  $\omega_e$  is regarded as constant within the sampling time step  $T_s$ , assuming that the electrical system's time constant is much smaller than the mechanical time constant. The motor inductances are assumed to be independent of currents. The time derivative can be expressed as:

$$\frac{\partial A}{\partial t} = \frac{A(t + \Delta t) - A(t)}{\Delta t} \quad (2)$$

where  $\Delta t$  is the time step taken between two successive time steps (two successive rotor's relative positions). Equation (1) can now be rewritten as:

$$\nabla \times (\nu \nabla \times A(t + \Delta t)) = \sigma \frac{\partial A(t + \Delta t)}{\Delta t} - \sigma \frac{\partial A(t)}{\Delta t} - J_z(t + \Delta t) + \nabla \times M_o(t + \Delta t) \quad (3)$$

The current/voltage sources related to the stator winding can be assigned either directly in the slot regions or through external electric circuit coupled to the regions. In a real drive system, the PM machine supplies or is fed through the three-phase current or voltage source. In order to determine the instantaneous value of the current density in each stator slot, the concept of space current vector and its relation to the MMF distribution is used. The armature current space vector  $\vec{i}_s$ , can be expressed in synchronous rotating frame as:

$$\vec{i}_s = I_m \cos(\varphi - \theta_{eo}) + jI_m \sin(\varphi - \theta_{eo}) \quad (4)$$

where,  $I_m$  is the peak value of the phase current,  $\varphi$  is the phase angle and  $\theta_{eo}$  is the initial angle between synchronous frame  $q$ -axis and phase- $a$  axis which carries maximum current at that instant. The coils  $a$ ,  $b$  and  $c$  of the circuit in the figure (2) represent stator phase windings which are defined by the coil resistance and number

of turns. Since the 2D FEM cannot represent effect of end-turn, the inductance related with it needs to be calculated separately by some empirical formula and the value is included in the electric circuit as a series inductance  $L_{end}$ .

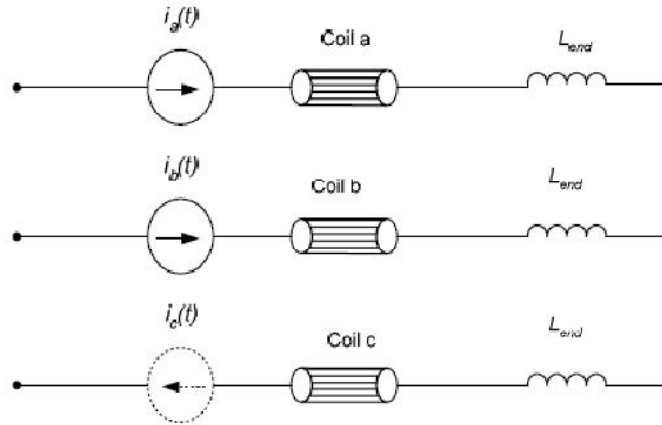


Figure (2): Coupled external circuit for the PM machine

The authors have developed a software package called the MCAD for the simulation purposes [9]. The MCAD software package provides the facilities to generate the mesh for the rotor and the stator of a machine and then combine the two meshes to generate the mesh for the whole machine. This feature is very helpful because a user can combine different rotors with different stators, also one can rotate the rotor mesh and then combine it with the stator mesh without the need to rebuild a new model for each case study. Once the FE models of the machine are generated, the MCAD's solver reads the machine data and some other information needed such as the stator and rotor current densities. The program first constructs the global reluctivity matrix, which is a set of system of non-linear equations, which are solved by Cholesky's method for nodal vector potential.

The post-processor of the software package MCAD provides the user with interactive computation and graphics visualization for the purpose of predicting the performance of the machines. Each FE solution provides the values of magnetic vector potential at every node. From this information the flux density, reluctivity, field intensity and energy of every element can be determined. The results obtained from the discrete time steps of the machines model are then used to predict the generator parameters and performance such as the induced EMF, stator reactance, torque and power, and the vector potential solution is used to plot lines of constant vector potential. Figure (3) shows some examples for the constant vector potential plots.

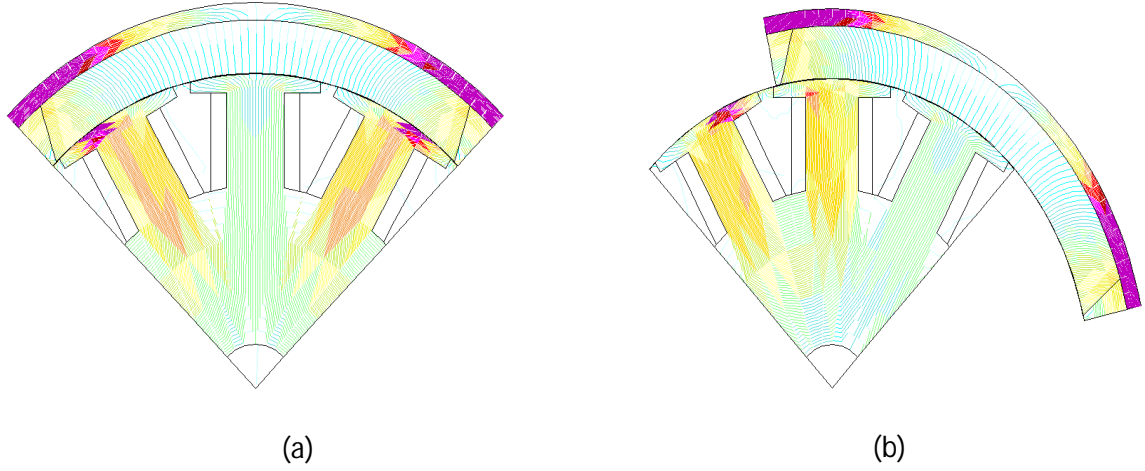


Figure (3): The flux plots of the prototype (a & b) one pole at different time steps.

**2-1- Induced Voltage Prediction**

The EMF induced in a machine is calculated from the Faradays’s law as:

$$E = -\omega \frac{d\phi}{dt} \tag{5}$$

Where  $\phi$  is the flux linkage over the effective tooth area (1/3 high from stator core),  $\omega$  is the speed and  $\theta$  is the rotor position in electrical degree. The flux  $\phi$  is related to flux-density as,

$$\phi = \int_s B ds \tag{6}$$

Hence

$$E = -\omega \frac{d}{dt} \left( \int_s B ds \right) = -\omega \int_s \frac{\delta B}{\delta t} \tag{7}$$

On the other hand, from Stoke’s theorem

$$E = \oint_l E_i dl = \int_s (\nabla \times E_i) ds \tag{8}$$

where,  $E_i$  is the induced electric field intensity. From the equations (7) and (8),

$$\nabla \times E_i = -\frac{\delta B}{\delta t} \tag{9}$$

The flux-density  $B$  in (9) can be expressed in terms of magnetic vector potential  $A$ . Therefore,

$$\nabla \times E_i = -\nabla \times \frac{\delta A}{\delta t} \tag{10}$$

$$\nabla \times \left( E_i + \frac{\delta A}{\delta t} \right) = 0 \tag{11}$$

Since *curl* of gradient is zero, the induced electric field intensity per unit length for one turn becomes,

$$E_i = -\frac{\delta A}{\delta t} \quad (12)$$

Integrating  $E_i$  over one stator teeth area, multiplying by number of turns and actual length of the machine, gives the induced EMF per phase as,

$$E = -\frac{lN_p h}{s} \int_s \frac{\delta A}{\delta t} ds \quad (13)$$

Here,  $A$  is determined from the time-stepping finite element method.

### Electromagnetic Torque Prediction

The Maxwell's stresses method is used to compute the electromagnetic torque. This method is the general computational method for the evaluation of electromagnetic force exerted at any surface that encloses the rotor, such as the air gap. This force is due to two principal stresses, the first type of these stresses is a tensile stress which acts along the flux lines, while the nature of the second type is compressive and acts at a normal direction to the flux lines. Normally in practical applications, it is more convenient to express these principle stresses in terms of the normal and tangential stress components. The tangential component is the only one of interest in the case of rotating electrical machines, since it is responsible for developing the electromagnetic force in the direction of rotation. While the normal component does not contribute to the torque development because of its resultant around the complete of the rotor cancels due to the symmetry. Periphery Electromagnetic force due to the tangential stress component is given by [14-15]:

$$F_t = \frac{1}{\mu^0} \oint B_n B_t ds \quad (14)$$

Where (s) is the surface of integration which is taken to be cylindrical, radius (r) is taken at the midway between the rotor and the stator elements to enclose the rotor [14-15]. In two dimensional treatments, the surface integral in equation (4-13) reduces to a line integral, and the equation then can be rewritten as:

$$F_t = \frac{rL}{\mu^0} \int_0^{2\pi} B_n B_t d\theta \quad (15)$$

Where  $ds$  is substituted by  $rLd\theta$ ,  $L$  is the effective axial length of the machine. The electromagnetic torque developed at this surface is:

$$T = \frac{r^2 L^2 \pi}{\mu^0} \int_0^{2\pi} B_n B_t d\theta \quad (16)$$

Direct implementation of equation (16) with finite elements method is very simple and it is not time consuming when the row of elements that represent the mid gap layer are labeled with special material code. The total electromagnetic torque over the path of integration can be found by summing the elemental torque contribution as follows:

$$T = \frac{2\pi r^2 L}{\mu^0} \sum_{e=1}^E B_{ne} B_{te} \quad (17)$$

Where  $E$  is the total number of air gap elements and  $(B_{ne})$  and  $(B_{te})$  are the normal and the tangential components of flux density evaluated at the centroid of each element.

**Inductance Prediction**

The synchronous inductance  $L_s$  can be determined from the field solution at each time step from the additional stored coenergy in the machine due to the magnetic field that resulted from the anature current [9, 16-18]. The finite element analysis is run first in normal non-linear model and then the model is linearized at the operating point for the parameter calculation. This is done by fixing the reluctivities for each element to correspond with the magnetic field distribution at the moment. After fixing the magnetic properties, an incremental current  $\Delta i$  is applied. The resulting change in the vector potential  $A$  is calculated from the linear system of equations. In this case, the reluctivity matrix holds the value from the last iteration step of the nonlinear solution. This ensures that the calculated inductance is incremental, thus representing the tangent of the magnetization curve. The incremental flux linkage  $\Delta\phi$  for all phase windings can be determined and hence  $L_s$ . The electromotive force ( $e$ ) is determined by subtracting the effect of the current derivative from the total flux derivative or from the knowledge of the winding arrangement. The total coenergy  $\Delta W$  can be found by the summation of all the incremental changes of elemental coenergies  $\Delta W_e$ . This incremental elemental coenergy can be fundamentally given by the following equation:

$$\Delta W_e = \int_{B_m}^{B_m+B_a} H dB \tag{18}$$

Where  $B_m$  is the flux density due to the field excitation and  $B_a$  is the flux density due to the armature winding current. After some manipulations on equation (18), the additional coenergy stored in each element can be given by:

$$\Delta W_e = \frac{B^2}{2\mu} \tag{19}$$

The total change in the coenergy  $W_m$  is then can be found by using the following relation:

$$\Delta W_m = \sum_{i=1}^E \Delta W_i L \tag{20}$$

Where (E) is the total number of elements and (L) is the axial length of the machine. From Equation (20), the synchronous reactance per phase can be given by the relation [19]:

$$X_s = \frac{4\Delta W_m}{3I^2} \omega L \tag{21}$$

Where  $\omega$  is the angular speed and I is the peak phase current.

The synchronous reactance that can be obtained from the last equation represents the total reactance including the leakage reactance. Leakage reactance is important to be total determined, and is classified into, slot leakage, Zig-zag leakage, end winding leakage and harmonics leakage. Only the first type can be obtained from the two dimensional treatment from numerical evaluation of the energy stored in the slots.

## Permanent Magnet Generator Performance

PM machines can operate as synchronous and brushless DC machines. In both cases, the machine consists of a stator, that have a single-phase or multi-phase winding which is sometimes called the armature winding, and a rotor that provides the main field of the machine by utilizing PMs. When the rotor rotates by a prime mover the magnetic flux vary by the angle rotation causing an induced EMF in the stator winding the output voltage is commutated to DC by the electronic rectifier.

PM machines allow a great deal of flexibility in their geometry. Based on the direction of flux penetration, permanent magnet machines can be classified as: radial flux [20], axial-flux [21], transversal-flux [22] and outer-rotor (or spindle) configurations [23]. In this paper an outer rotor (spindle) PM synchronous generator is used.

Figure (4) shows a simple block diagram of a BLDC PM generator. The system consists of a prime mover, three-phase PM generator, six switches rectifier (controlled or uncontrolled) and a controller and measurement system. The experimental setup consists of a 0.2kW, 1.0A, three-phase, four-pole PM BLDC generator drive connected with a permanent magnet DC motor as a prime mover, three-phase bridge rectifier and load. The parameters of PM generator machine are listed in table. Figure (5) shows the developed experimental BLDC generator system.

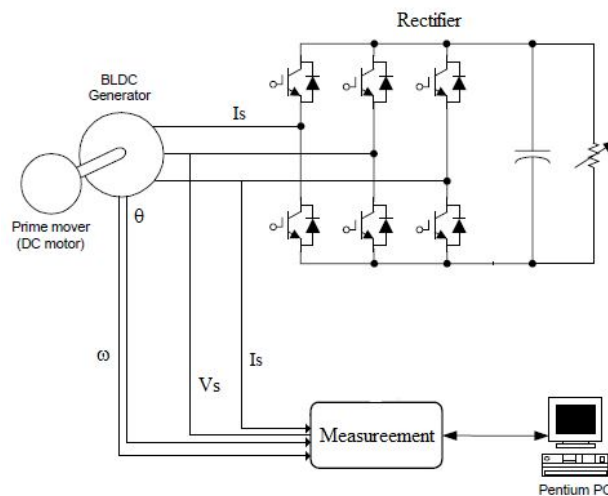


Figure (4): Block schematic of the experimental system.

The measurement system is responsible for measuring the line and phase voltages, line current, the speed, the power factor and the induced line and phase voltages. The line and phase induced voltages are measured with the aid of three phase dummy windings. Were used to measure the. The dummy windings are a single turn open circuited winding designed to have the same layout of the main armature winding. The generated voltage in the dummy winding represents the air-gap induced voltage in the generator. The speed of the generator is measured with the aid shaft encoder. For voltage sensing, a Hall-effect voltage sensor, which is also manufactured by the

LEM (LV25-P) is used. The entire drive system is controlled by using the PIC 16f877 micro-controller. The micro-controller has a high-speed 10-bit Analog-to-Digital (A/D) converter which has four independent channels.



Figure (5): The experimental set-up

Table (1): Specification of the BLDC generator

Poles	4	Resistance	4.3 Ω
Phase	3	Inductance	4.3 mH
Power	0.2 kW	$K_e$	1.29 V/rps
DC-link Battery	24 V	Rated Current	1 Amp

### Performance Evaluation for the Synchronous Generator

This section presents the performance analysis of the PM generator when operated as a synchronous generator. Simulation results obtained by using time-stepping FEA are compared with those obtained experimentally.

When a synchronous machine is operated as a synchronous generator, as shown in figure (6), a prime mover is required to drive it. In steady state, the mechanical torque of the prime mover should balance with the electromagnetic torque produced by the generator and the mechanical loss torque due to friction and windage, or

$$T_{IN} = T_{em} + T_{Loss} \tag{22}$$

Multiplying the synchronous speed to both sides of the torque equation, we have the power balance equation as

$$P_{IN} = P_{em} + P_{Loss} \tag{23}$$

where  $P_{IN} = T_{IN} \omega_{syn}$  is the mechanical power supplied by the prime mover,  $P_{em} = T_{em} \omega_{syn}$  the electromagnetic power of the generator, and  $P_{loss} = T_{loss} \omega_{syn}$  the mechanical

power loss of the system. The electromagnetic power is the power being converted into the electrical power in the three phase stator windings. That is

$$P_{em} = T_{em} \omega_{syn} = 3 E_a I_a \cos \varphi_i \quad (24)$$

where  $\varphi_i$  is the angle between phasors  $E_a$  and  $I_a$  and it is called the internal power factor.

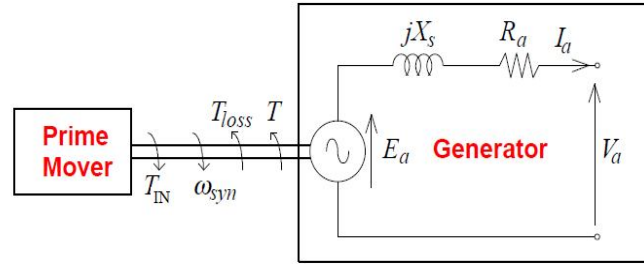


Figure (6): PM machine equivalent circuit when operating as generator

For small PM synchronous generators, the winding resistance is generally is not smaller than the synchronous reactance as in large synchronous generators, and thus the per phase circuit equation is written as:

$$E_a = V_a + I_a R_a + j I_a X_s \quad (25)$$

The corresponding phasor diagram is shown in figure (7). From the phasor diagram, we can readily obtain that:

$$E_a \sin \theta = X_s I_a \cos \theta - R_a I_a \sin \theta \quad (26)$$

where  $\theta$  is the angle between the phasors of the voltage and the EMF known as the *load angle*.

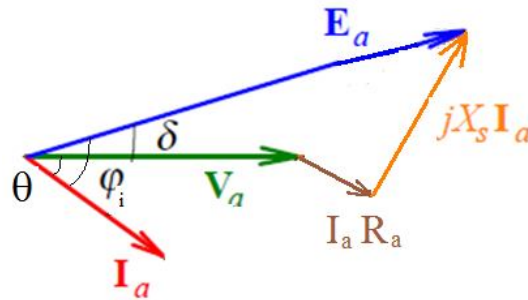


Figure (7): PM machine phasor diagram when operating as generator

In this work only resistive load is applied, thus apparent power factor angle  $\theta$  is zero from which the internal power factor will then equal the load angle and hence equation (27) is rewritten as:

$$E_a \sin \theta = X_s I_a \cos \theta \quad (27)$$

The output electrical power equals the electromagnetic power, or

$$P_{em} = P_{out} = 3 V_a I_a \cos \theta_i \quad (28)$$

Therefore,  $\theta$  can also be regarded as the angle between the rotor and stator rotating magnetic fields. The electromagnetic torque of a synchronous machine is proportional to the sine function of the load angle.

The, terminal voltage and current of the generator at steady state were measured for rated speed and various load conditions. Figures (8) and (9), show (a) the generator line voltage and induced EMF for two different load resistors ( $R = 50\Omega$ , and  $R = 70\Omega$ ) at a speed of 1250r/min. Tables (2) and (3) presents the measured and computed results respectively obtained for different load resistance. It can be concluded from these figures that an excellent agreement between the measured and computed results by the FEM exists.

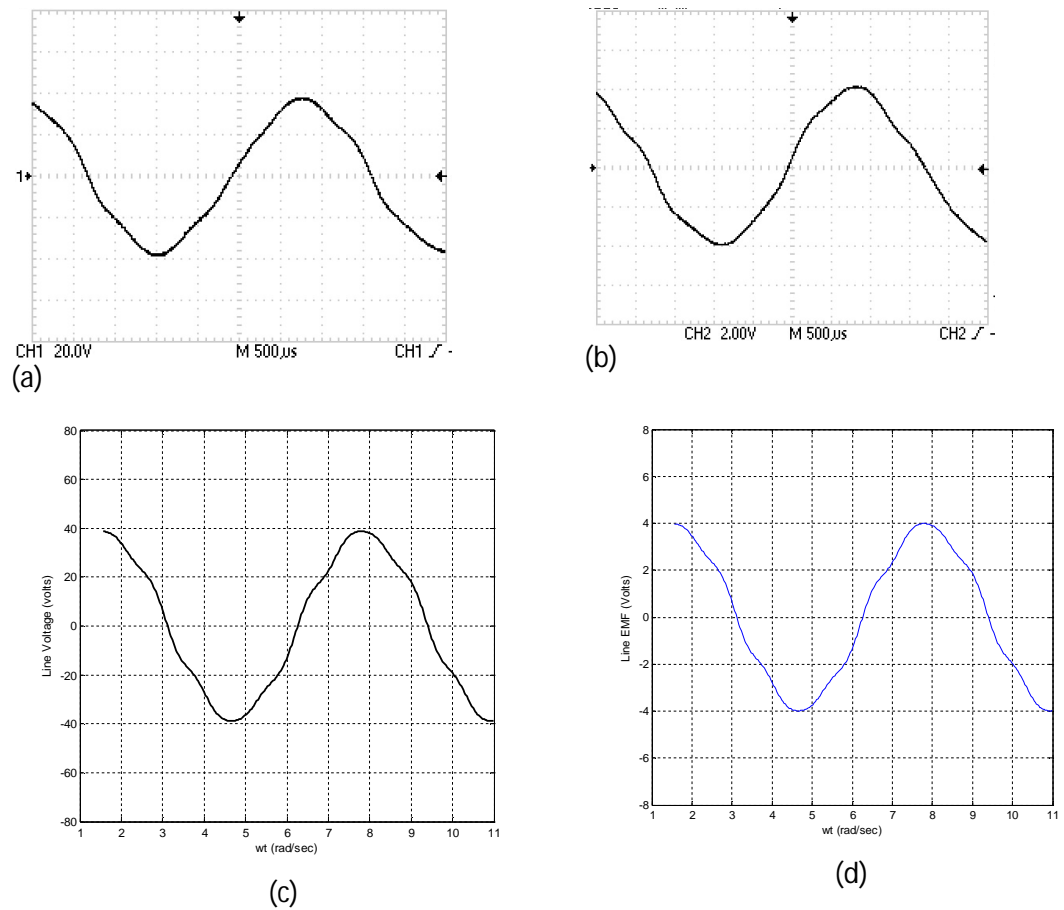


Figure (8): Comparison between computed and measured line voltage and induced EMF for  $R_{Load} = 50\Omega$ ; (a) Measured line voltage; (b) Measured line EMF; (c) Computed line voltage; (d) Computed line EMF.

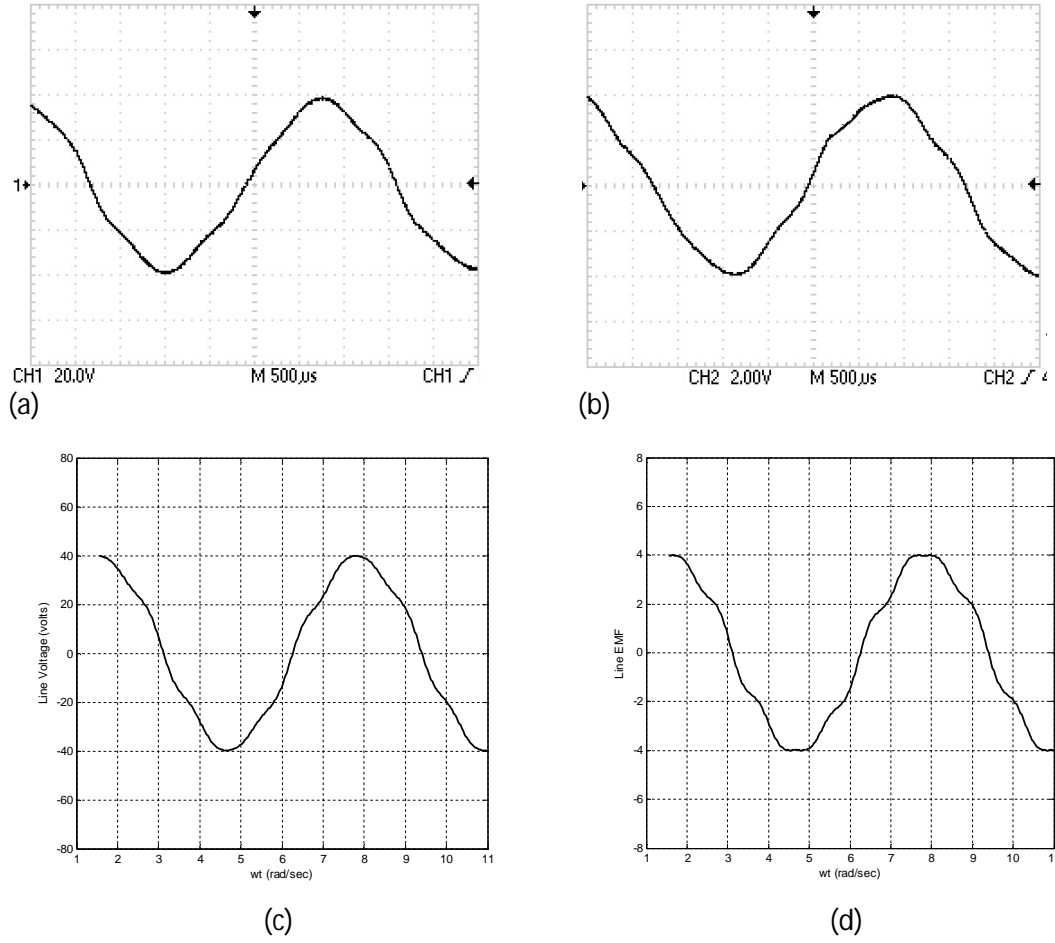


Figure (9): Comparison between computed and measured line voltage and induced EMF for  $R_{Load} = 70\Omega$ ; (a) Measured line voltage; (b) Measured line EMF; (c) Computed line voltage; (d) Computed line EMF.

**Table 2:** Measured steady-state performance parameters

Load Resistance $\Omega$	Line Current (Amp)	Phase Voltage (Volts)	Phase EMF (Volts)	Power factor angle	Load angle (degrees)
20	0.64	14.29	1.22	1.03	5.32
30	0.45	14.70	1.33	1.03	5.14
40	0.35	14.95	1.36	1.03	5.04
50	0.28	15.31	1.45	1.03	4.89
60	0.24	15.92	1.47	1.04	4.63
70	0.2	16.33	1.49	1.04	4.12

**Table 3:** Computed steady-state performance parameters

Load Resistance $\Omega$	Line Current (Amp)	Phase Voltage (Volts)	Phase EMF (Volts)	Power factor angle	Load angle (degrees)
20	0.64	14.4	1.29	1.00	5.22
30	0.45	14.95	1.39	1.00	5.07
40	0.35	15.23	1.42	1.00	4.98
50	0.28	15.61	1.63	1.00	4.92
60	0.24	16.15	1.67	1.00	4.79
70	0.2	16.73	1.68	1.00	4.31

**Performance Evaluation for the BLDC Generator**

This section presents the steady state performance of the PM machine operating as a BLDC generator. The performance characteristics of the machine as a BLDC generator was measured and compared with the predicted values of FE model. The main difference between the operation of the PM generator as a three-phase synchronous generator and as a BLDC generator is the integration of three-phase rectification unit. The rectifier with the filtering capacitor as been stated converts the three phase voltage obtained from the PM synchronous generator to DC voltage. Although, resistive loads are connected to the output of the rectifier but the addition of the rectifier unit will affect the nature of the load from the point view of the generator. This means that the generator will be subjected to a non-unity power factor load as in that considered in the previous section. The power factor of the rectifier unit and the load depends on the internal characteristics of the diodes, the filtering capacitor and the resistive load. The power factor is measured by measuring the difference between the current and phase voltage waveforms. In order to perform an accurate prediction for the generator performance under different loading conditions, the current density in each phase winding must be calculated accurately. The value of the current density for each position of the rotor is calculated from the knowledge of the output current, the power factor and the load angle. The load angle as stated before is measured from the phase difference between the phase voltage and the induced phase voltage. The power factor is calculated from the phase difference between the phase voltage waveform and the generator current waveform. By knowing these two values, the instantaneous value of the current and with the aid of phasor diagram shown in figure (10), we can find the instantaneous value of the current density in each phase from which then the other parameters can be predicted. Figure (11) shows the generator current waveform under full load condition and speed of 1200r/min. Figure (12) shows the variation of the load angle and figure (13) shows the power factor for different load values.

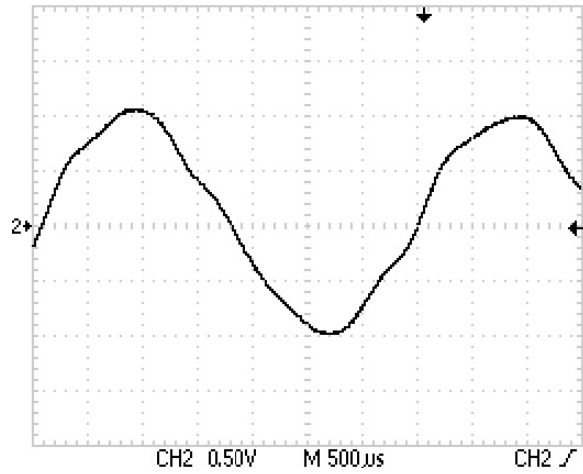


Figure (10): Generator output current waveform at full load.

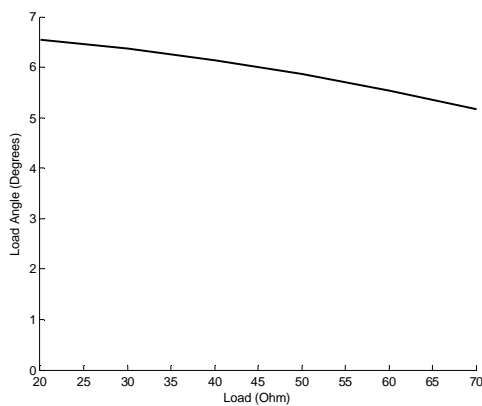


Figure (11): Variation of load angle with the load resistance.

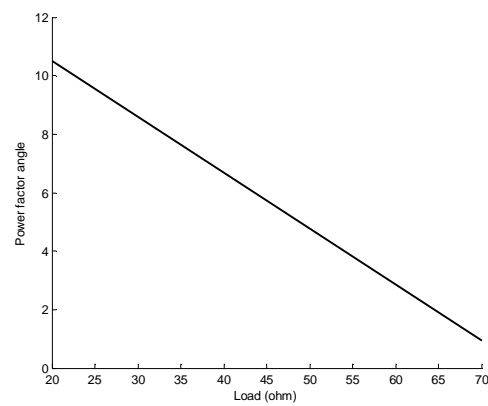


Figure (12): Variation of power factor angle with the load resistance.

The DC bus voltage, terminal voltage and current of the generator at steady state were measured for various speed and load conditions. Figure (13), figure (14) and figure (15) show the line voltage, the induced voltage and the DC bus voltage respectively for the full load condition at a speed of 1250r/min.

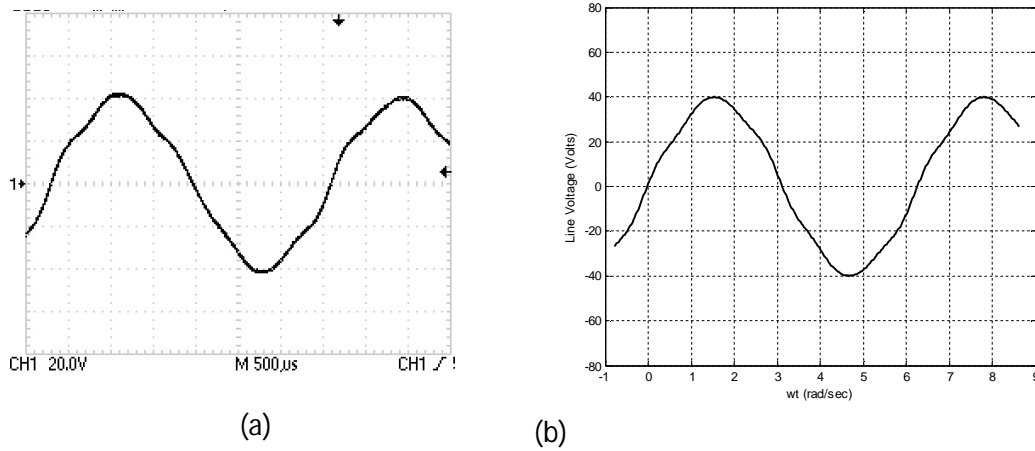


Figure (13): Line voltage at full load and speed = 1250r/min (a) measured, (b) FE computed

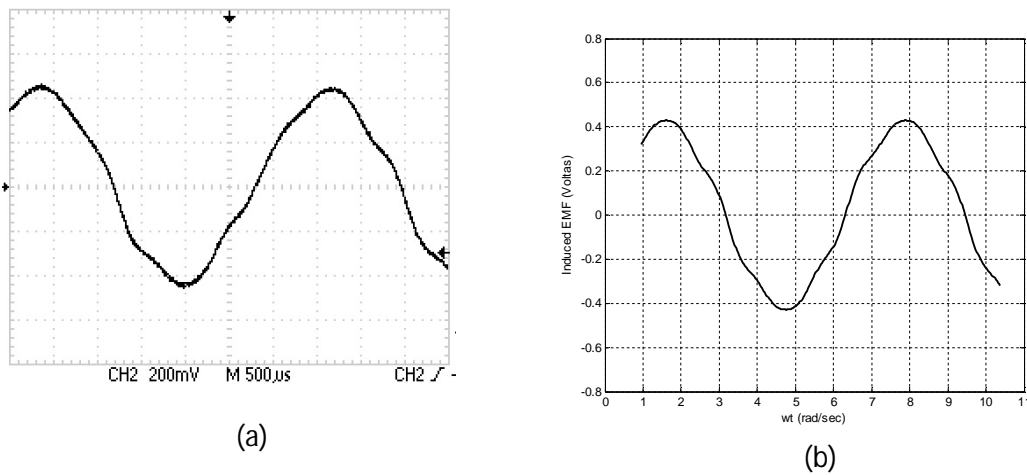


Figure (14): Line induced EMF at full load and speed = 1250r/min (a) measured, (b) FE computed

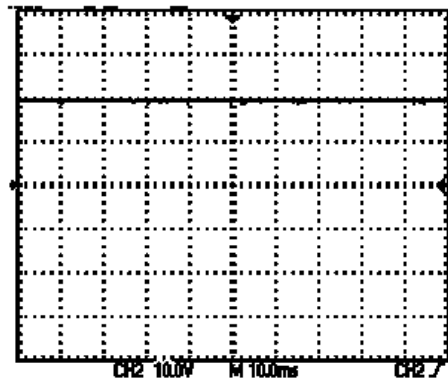


Figure (15): Measured DC bus voltage at full load and speed of 1250 r/min

The power-speed capability of the generator at various speeds were measured and compared to the predicted values obtained from the finite element model. The machine operates in the third quadrant of the dq plane during generation [22]. Hence, in the finite element analysis, the current angle was varied between 90 to 180 electrical degrees. The figure (16) shows the predicted and measured power capability of the generator up to the speed 2800 r/min. Again, measured values were found to closely match the predicted ones. The power remains nearly constant from 2400 r/min to the 2800 r/min.

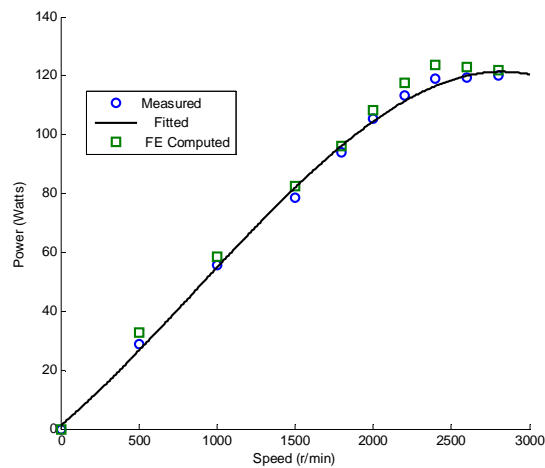


Figure (16): Power capability curve of the PM generator

## Conclusions

The outer-rotor PM generator described in the paper is used for a standalone application either running as generator or brushless DC generator. It is verified that a PM generator made in such a simple construction can operate with good and reliable performance over a wide range of speeds. The simulation of PM BLDC generator using time stepping FEM will be presented and is compared with those obtained from a small outer rotor PM generator prototype. The comparison between the results obtained from the FE model and those obtained experimentally shows the validity of the FEM to analyze PM BLDC generators.

## References

- [1] F. Dastgeer, and A. Kalam : “Efficiency comparison of DC and AC distribution systems for distributed generation”; Australasian Universities Power Engineering Conference, 2009. AUPEC 2009; 2009; pp. 1–5.
- [2] Z. Chen and E. Spooner, “Wind Turbine power Converters: a Comparative Study,” Seventh International Conference of IEE Power Electronics and Variable Speed Drives, 1998, pp. 471 – 476.
- [3] Duane Hanselman: “Brushless permanent magnet motor design 2nd ed”; Magna Physics Publishing; Ohio USA, 2006.

- [4] Hyung-Woo Lee; Tae-Hyung Kim and M. Ehsani: "Practical control for improving power density and efficiency of the BLDC generator"; IEEE Trans. on Power Electronics; Vol. 20, Issue 1, 2005, pp.
- [5] Q. Deng, G. Liu and F. Xiao: "Control of variable-speed permanent magnet synchronous generators wind generation system"; International Conference on Electrical Machines and Systems, 2008. ICEMS 2008; pp. 2454 - 2458.
- [6] S. G. Burrow, P. H. Mellor, P. Churn, T. Sawata and M. Holme: "Sensorless Operation of a Permanent-Magnet Generator for Aircraft"; IEEE Trans. on Industry Applications; Vol. 44; Issue 1; 2008; pp. 101 – 107.
- [7] Zhang Xueyi and Shi Liwei: "Study on Controlled Rectification Constant-Voltage Permanent-Magnet Rare Earth Generator of Hybrid Vehicles"; Second International Conference on Intelligent Computation Technology and Automation, 2009. ICICTA '09; Vol. 1, 2009, pp. 898-901.
- [8] C.M. Ong: "Dynamic Simulation of Electric Machinery Using MATLAB /SIMULINK" Upper Saddle River, NJ: Prentice Hall PTR, 1998.
- [9] Munaf S. N. Al-Din: "Computer Aided Analysis and Design Optimization of High Speed Permanent Magnet Synchronous Motors"; Ph.D. Dissertation, University of Technology Baghdad-Iraq, 1997.
- [10] M. A. Jabbar, , Zhejie Liu, and Jing Dong: Time-Stepping Finite-Element Analysis for the Dynamic Performance of a Permanent Magnet Synchronous Motor, IEEE Transactions on Magnetics, Vol. 39, No. 5, Sept. 2003, pp. 2621-2623.
- [11] Joao Pedro A. Bastos and Nelson Sadowski : "Electromagnetic Modelling by Finite Element methods"; Marcel Dekker, Inc. 2003.
- [12] De Gersem, H., Mertens, R., Lahaye, D., Vandewalle, S., and Hameyer, K.: "Solution Strategies for Transient, Field-Circuit Coupled Systems", IEEE Transactions on Magnetics, Vol. 36, No. 4, July 2000, pp. 1531–1534.
- [13] W. N. Fu, Zheng Zhang, P. Zhou, D. Lin, S. Stanton and Z. J. Cendes: "Curvilinear finite elements for modeling the sliding surface in rotating electrical machines and its applications"; IEEE International Conference on Electric Machines and Drives IEMDC.2005, 2005, pp. 628-634.
- [14] A. N. Wignall, A.J. Gilbert and S.J. Yang, Calculation of forces on magnetised ferrous cores using the Maxwell stress method, IEEE Trans. on Magnetics, Vol. 24, No. 1, 1988, pp.459-462.
- [15] K. Komez, A. Pelikant, J. Tegopoulos and S. Wiak, Comparative Computation of Forces and Torques of Electromagnetic Devices by Means of Different Formulae, IEEE Trans. on Magnetics, Vol. 30, No. 5, 1994, pp.3475-3478.
- [16] T. W. Nehl, F. A. Fouad, and N. A. Demerdash, "Determination of saturated values of rotating machinery incremental and apparent inductances by an energy perturbation method," IEEE Trans. Power Appart. Syst., vol. 101, no. 12, pp. 4441–4451, 1982.
- [17] Liuchen Chang, An Improved FE Inductance Calculation for Electrical Machines, IEEE Trans. on Magnetics, Vol 32, No. 4, July 1996, pp. 3237-3245.

- [18] Jacek F. Gieras, Ezio Santini, and Mitchell Wing, Calculation of Synchronous Reactances of Small Permanent-Magnet Alternating-Current Motors: Comparison of Analytical Approach and Finite Element Method with Measurements, *IEEE Trans. on Magnetics*, Vol. 34, No. 5, Sept. 1998, pp.3712-3720.
- [19] P.H. Mellor, F.B. Chaaban, K.J. Binns, "Estimation of Parameters and Performance of Rare-Earth Permanent-Magnet Motors Avoiding Measurement of Load Angle," *IEE Proceedings-B*, Vol. 138, No. 6, Nov. 1991, pp. 322-330.
- [20] M. Joorabian and A. Z. Nejad: "Design and construction of an optimum high power radial flux direct-drive PM generator for wind applications"; 4th IEEE Conference on Industrial Electronics and Applications, 2009. ICIEA 2009; 2009, pp. 524-529.
- [21] A. Parviainen, J. Pyrhonen and P. Kontkanen: " Axial Flux Permanent Magnet Generator with concentrated Winding for Small Wind Power Applications"; *IEEE International Conference on Electric Machines and Drives, IEMDC.2005; 2005*; pp. 1187-1191.
- [22] F. Jacek, "Performance characteristics of a transverse flux generator"; *IEEE International Conference on Electric Machines and Drives, IEMDC'2005; 2005*; pp. 1293-1299.
- [23] Xing-jia Yao,; Lei Tia, Zuo-xia Xing, Ke Li and Xian-bin Su:" Study on a New Control Strategy of Inverter of Outer Rotor Permanent Magnet Generator Wind Power System"; *International Conference on Energy and Environment Technology, ICEET '09; Vol. 1, 2009*, pp. 833-836.